



HAL
open science

Shape transition in InAs nanostructures formed by Stranski-Krastanow growth mode on InP (001) substrate

Anne Ponchet, Laurent Pedesseau, Alain Le Corre, Charles Cornet, Nicolas Bertru

► To cite this version:

Anne Ponchet, Laurent Pedesseau, Alain Le Corre, Charles Cornet, Nicolas Bertru. Shape transition in InAs nanostructures formed by Stranski-Krastanow growth mode on InP (001) substrate. Applied Physics Letters, 2019, 114 (17), pp.173102. 10.1063/1.5091058 . hal-02119035

HAL Id: hal-02119035

<https://hal.science/hal-02119035v1>

Submitted on 26 Jul 2022

HAL is a multi-disciplinary open access archive for the deposit and dissemination of scientific research documents, whether they are published or not. The documents may come from teaching and research institutions in France or abroad, or from public or private research centers.

L'archive ouverte pluridisciplinaire **HAL**, est destinée au dépôt et à la diffusion de documents scientifiques de niveau recherche, publiés ou non, émanant des établissements d'enseignement et de recherche français ou étrangers, des laboratoires publics ou privés.

Shape transition in InAs nanostructures formed by Stranski-Krastanow growth mode on InP (001) substrate

Cite as: Appl. Phys. Lett. **114**, 173102 (2019); <https://doi.org/10.1063/1.5091058>

Submitted: 01 February 2019 . Accepted: 24 March 2019 . Published Online: 03 May 2019

Anne Ponchet, Laurent Pedesseau , Alain Le Corre, Charles Cornet, and Nicolas Bertru



View Online



Export Citation



CrossMark

Applied Physics Reviews
Now accepting original research

2017 Journal
Impact Factor:
12.894

AIP
Publishing

Shape transition in InAs nanostructures formed by Stranski-Krastanow growth mode on InP (001) substrate

Cite as: Appl. Phys. Lett. **114**, 173102 (2019); doi: [10.1063/1.5091058](https://doi.org/10.1063/1.5091058)

Submitted: 1 February 2019 · Accepted: 24 March 2019 ·

Published Online: 3 May 2019



View Online



Export Citation



CrossMark

Anne Ponchet,¹ Laurent Pedesseau,²  Alain Le Corre,² Charles Cornet,² and Nicolas Bertru^{2,a)}

AFFILIATIONS

¹CEMES, Université de Toulouse, CNRS, 29 Rue Jeanne Marvig, F-31055 Toulouse, France

²Univ Rennes, INSA Rennes, CNRS, Institut FOTON-UMR 6082, F-35000 Rennes, France

^{a)} Author to whom correspondence should be addressed: nicolas.bertru@insa-rennes.fr.

ABSTRACT

The shape of InAs nanostructures formed by molecular beam epitaxy on a (001) InP substrate in the Stranski-Krastanow growth mode is studied. A transition from wires to round-shaped islands is observed as a function of the amount of InAs deposited. It is attributed to the non-equivalent energies of the A and B facets existing in zinc blende materials (facets along $[1\bar{1}0]$ and $[110]$, respectively). This surface energy anisotropy is considered to determine the nanostructure equilibrium shape from the balance between the elastic energy and the surface energy. At low volumes, the most energetically favorable shape is the wire-like shape, while at high volumes, the equilibrium shape is the island-like shape. The calculated sizes for which the shape changes are in good agreement with experimental sizes. The low lattice mismatch and the low surface energy of (114)A InAs facets around $41 \text{ meV}/\text{Å}^2$, as obtained from density functional theory calculations, enhance this effect in the InAs/InP system.

Published under license by AIP Publishing. <https://doi.org/10.1063/1.5091058>

Self-assembled InAs nanostructures (NSs) formed by Stranski-Krastanow (SK) growth mode on InP (001) substrates have received renewed interest for $1.55 \mu\text{m}$ optical telecom devices. Already, lasers,¹ mode-locked lasers,² and semiconductor optical amplifiers (SOA)³ have been achieved with improved performances (see the recent review in Ref. 4). In contrast with the InAs/GaAs material system, the deposit of a few monolayers (MLs) of InAs by molecular beam epitaxy (MBE) on InP(001) leads to the formation and the undesirable coexistence of nanostructures presenting various shapes, including wires, dashes and round-shaped islands.^{5,6} Due to the importance of NS shape in device elaboration,⁷ systematic studies have been conducted to control their morphology, including As_2 over As_4 molecules during InAs deposition,⁸ or the nature of the buffer layer (GaInAs, InP, and AlInAs).⁹ Shape transitions from wires to islands were observed with the amount of InAs deposited¹⁰ or the growth interruption time.¹¹ Most interpretations on shape changes are based on a large indium adatom diffusion anisotropy and the low lattice mismatch between InAs and InP (3.2%),⁹ but a complete picture of InAs NS formation on InP (001) is lacking and the mechanisms which govern their size and shape evolution are not yet fully understood.

In other materials systems such as Ge/Si(001) and InAs/GaAs (001), the formation of NSs with various shapes has also been reported.¹² In particular, a shape change as a function of NS volume from flat huts to sharper domes was observed.¹³ This shape transition was explained by the energy balance between the elastic relaxation allowed by the NS and the surface energy cost induced by facet formation. As the surface and elastic energies scale, respectively, with the square and the cube of the island size,¹⁴ the NS shape for small structures is mainly controlled by the minimization of surface energy cost, and for larger NSs by high strain relaxation allowed by taller and sharper structures. However, the NS shape in these systems is isotropic without elongation in a crystallographic direction, unlike it is observed in the InAs/InP system.

In this paper, we present experimental evidence that a transition from elongated structures to round-shaped islands occurs in the InAs/InP (001) system with the increase of deposited InAs. To account for this transition, we calculated the energy gain associated with the NS formation as a function of the NS shape and volume. In contrast with previously reported models, we consider different surface energies for facets along $[1\bar{1}0]$ and $[110]$ crystallographic directions (A and B facets, respectively). Indeed, in contrast with silicon and germanium,

polar III–V compounds crystallize in a zinc blende structure, and (11n)A and (11n)B crystallographic planes present different atomic arrangements and thus different surface density energies. We estimated surface energies from density functional theory (DFT) and the elastic energy relaxation by the finite element method (FEM) in the frame of anisotropic elasticity theory. We determined the NS equilibrium shape as a function of volume. The role of surface energy anisotropy in the evolution from elongated to rounded NSs is thus discussed in the case of moderate lattice mismatch existing in the InAs/InP system ($\Delta a/a = 3.2\%$).

All samples were elaborated by gas source MBE. After oxide desorption at 525 °C, the substrate temperature was reduced at 480 °C. Then, a 0.3 μm InP buffer layer was deposited, followed by a 100 nm thick $\text{Ga}_{0.2}\text{In}_{0.8}\text{As}_{0.435}\text{P}_{0.665}$ alloy layer, lattice matched with InP and used to achieve optical confinement in InP-based devices. Lattice matching condition of the quaternary alloy was checked by high resolution X-ray diffraction. After a growth interrupt (GI) of 10 s under As and P fluxes and of 5 s under an As flux, NS formation was initiated on the GaInAsP surface by InAs deposition at 0.33 ML/s with an As beam equivalent pressure of 0.9×10^{-7} Torr. During whole growth runs, group V-rich surface reconstructions were observed. After NS formation, a 30 s GI under As was performed at 480 °C, and then the samples were cooled down quickly to room temperature. Atomic force microscopy (AFM) measurements were performed in contact mode.

Deposits of various amounts of InAs were examined by AFM (Fig. 1). The structural characteristics of the NS are reported in Table I. With the deposition of 2.1 ML of InAs, a value slightly higher than the critical thickness for transition from the two-dimensional (2D) mode to the 3D growth SK mode, structures elongated along $[\bar{1}10]$ with a low height (<1 nm) are observed. The spatial organization is low with a large dispersion in the length and the width. The wires obtained after 2.8 ML deposition present a better spatial organization, a larger length (>180 nm) and height (1 nm), while the size dispersion is considerably reduced. The wires cover most of the surface. For 3 ML

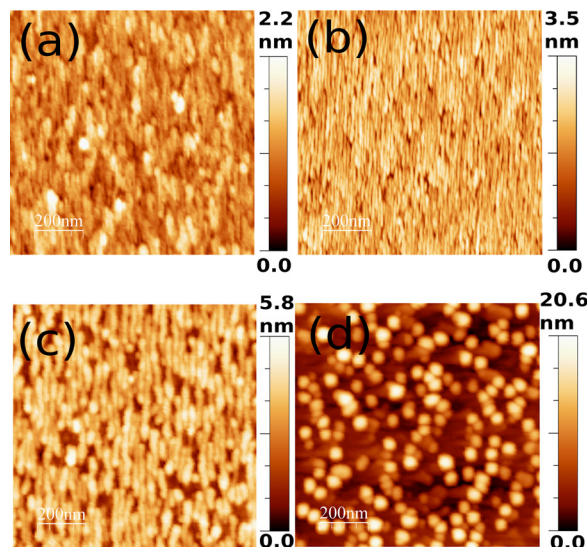


FIG. 1. $1 \mu\text{m} \times 1 \mu\text{m}$ AFM images after the deposition of 2.1 ML (a), 2.8 ML (b), 3 ML (c), and 3.5 ML (d) of InAs.

TABLE I. Structural characteristics of InAs nanostructures, as deduced from AFM measurements.

Thickness	2.1ML	2.8ML	3ML	3.5ML
Type	Mix	Wire	Wire + island	Island
Height (nm)	0.5–1	1–1.2	2.6	9.2
Width (nm)	30	10	35	65
Length (nm)	100	>180	>140	65

deposition, a mix of wires and round-shaped islands are observed. At the extremity of the wires, round-shaped islands are observed. For 3.5 ML, a drastic change in AFM images is observed. Only round-shaped islands are obtained, with a low density. Thus, as the deposited InAs amount increases, a change from wire-shaped structures of low height and elongated along $[\bar{1}10]$ to large and round-shaped islands with a larger height is observed. This transition occurs around 3 ML with dispersion from one sample to other ones, despite the same nominal growth conditions. AFM scans perpendicular to facets reveal that the facets parallel to $[1\bar{1}0]$ are systematically (114)A [at 19.6° inclination to the (001) surface]. Facets along the $[110]$ direction (B type) are considerably less developed, with an angle around 18° at the end of the wires and around 23° for large round-shaped islands. Similar results were reported by other groups with typical lateral dimensions of wires around 25–30 nm along $[110]$, 100 to 800 nm along $[\bar{1}10]$ and height around 1–3 nm. The round-shaped islands are usually higher (5–8 nm typically).⁶ (114)A facets are repeatedly reported.^{15,16}

To account for this transition, we propose to calculate the total NS formation energy cost, considering surface energy anisotropy. The NS is modeled as a wire of height (h) with a rectangular base of length (L) and width (w) along the $[\bar{1}10]$ and $[110]$ directions, respectively [Fig. 2(a)]. The NS facets parallel to $[\bar{1}10]$ and $[110]$ consist of (11m)A and (11n)B crystallographic planes, respectively. The facet angles with (001) planes are α and β , respectively, with $\alpha \leq \beta$ as experimentally observed (i.e., $m \geq n$). The island shape is fully characterized by the dimensionless elongation and truncation ratios, e and t , respectively, defined by

$$e = \frac{L}{w} \quad \text{and} \quad t = 1 - \frac{2h}{w \tan \alpha}$$

t scales from 0 (untruncated NS) to 1 (fully truncated NS i.e., 2D morphology); $e > 1$ means an elongation along $[\bar{1}10]$, while $e < 1$ means an elongation along $[110]$.

The total energy cost for NS formation relative to a 2D layer of same volume V is the sum of a bulk strain relaxation contribution E_V and a surface term E_S .¹⁴ The gain of the bulk elastic energy E_V due to the SK growth mode is

$$E_V = -R e_{2D} V, \quad (1)$$

$$e_{2D} = \left(C_{11} + C_{12} - 2 \frac{C_{12}^2}{C_{11}} \right) \varepsilon^2, \quad (2)$$

where e_{2D} is the volume density of the elastic energy of a 2D strained layer with an in-plane strain ε ($\varepsilon \approx -\Delta a/a$). For InAs, the elastic coefficients C_{11} , C_{12} , and C_{44} are 84.4, 46.4, and 39.6 GPa, respectively.¹⁷ R is the relaxation factor depending on the NS geometry. It can be numerically calculated by FEM.¹⁸ It is null for a 2D strained layer that

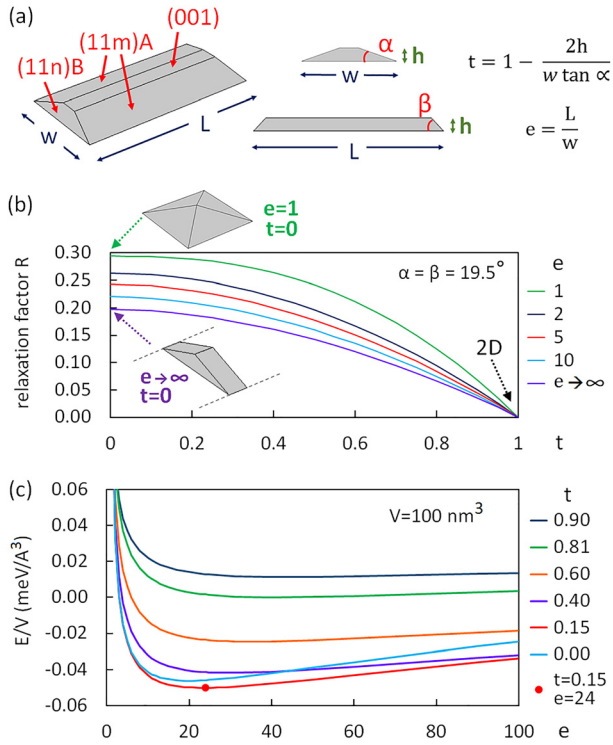


FIG. 2. (a) Scheme of the modeled NS and definitions of the aspect ratios t and e , describing, respectively, the NS truncation and elongation. (b) Relaxation factor calculated by FEM as a function of t and e for $\alpha = \beta = 19.5^\circ$. (c) Energy per volume unit as a function of e and t for a particular volume $V = 100 \text{ nm}^3$, and surface energies of 47.0 , 44.5 , and $49.0 \text{ meV}/\text{Å}^2$ for (001), (114)A and (114)B facets, respectively ($\alpha = \beta = 19.5^\circ$). The red dot indicates the minimum energy, achieved with $e = 24$ and $t = 0.15$.

corresponds here to the truncation ratio $t = 1$. For a given α and β , R increases as t decreases and/or the elongation ratio e gets closer to $\tan \alpha / \tan \beta$. R is maximal when $e = \tan \alpha / \tan \beta$ and $t = 0$ (the steepest nontruncated NS).

In the SK growth mode, the cost of surface energy E_S for NS formation compared to the 2D layer depends on the contact area ($S = Lw$) between the NS and the wetting layer, the areas of the (11m)A, (11n)B and top (001) facets (S_A , S_B , and $S_{(001)}$, respectively) and their respective surface energy densities $\gamma_{(11m)A}$, $\gamma_{(11n)B}$, and $\gamma_{(001)}$

$$E_S = \gamma_{(11m)A} S_A + \gamma_{(11n)B} S_B + \gamma_{(001)} (S_{(001)} - S). \quad (3)$$

It is convenient to introduce the effective surface energy density γ_S defined by $E_S = \gamma_S S$. It comes from Eq. (3)

$$\gamma_S = \frac{1-t}{e} \left(e + (t-1) \frac{\tan \alpha}{2 \tan \beta} \right) \left(\frac{\gamma_{(11m)A}}{\cos \alpha} - \gamma_{(001)} \right) + \frac{1-t^2}{e} \frac{\tan \alpha}{2 \tan \beta} \left(\frac{\gamma_{(11n)B}}{\cos \beta} - \gamma_{(001)} \right). \quad (4)$$

The stability of the (001) surface (in the absence of the strain relaxation effect) against (11m)A and (11n)B faceting requires that $\gamma_{(11m)A} / \cos \alpha$ and $\gamma_{(11n)B} / \cos \beta$ are larger than $\gamma_{(001)}$.

The surface energy density of stable InAs (001) surfaces was estimated from DFT by several groups.^{19–21} For the $\beta 2(2 \times 4)$ reconstruction, it varies from $44 \text{ meV}/\text{Å}^2$ (As-rich conditions) to $51 \text{ meV}/\text{Å}^2$ (Ga-rich conditions), while for the stoichiometric $\alpha 2(2 \times 4)$ one, it is close to $48 \text{ meV}/\text{Å}^2$. Here, we arbitrarily consider an intermediate value of $47 \text{ meV}/\text{Å}^2$. For A facets, we consider $\alpha = 19.5^\circ$ from the experimental observations of (114)A facets. The InAs (114)A surface energy calculations or measurements are lacking. A model of the stable stoichiometric $\alpha 2(2 \times 1)$ reconstruction was proposed for the GaAs (114)A surface.²² Using DFT as implemented in the SIESTA package, we calculated the surface energy of an InAs (114)A surface, $\alpha 2(2 \times 1)$ reconstructed. Calculation details were already described elsewhere.²³ A $\gamma_{(114)A}$ of $41 (\pm 5) \text{ meV}/\text{Å}^2$ was obtained. This low value agrees with the high stability of the (114)A InAs surfaces observed experimentally.²⁴ Nevertheless, it could lead to an instability of the (001) InAs surface which is not observed experimentally. In the following, we chose $\gamma_{(114)A} = 44.5 \text{ meV}/\text{Å}^2$, within the accuracy range of the DFT result, but preserving the stability of InAs(001).

For facets parallel to [110] directions, there are no evidence in the literature for the existence of stable (11n)B surfaces with a high n index. The (111)B InAs surface is a stable surface and its energy $\gamma_{(111)B}$ calculated by DFT is about 1 to 1.15 times of $\gamma_{(001)}$ in the As-rich range of variation of the As chemical potential.²¹ Given the experimental observations, we consider here facets with $\beta = 19.4^\circ$ corresponding to (114)B and a surface energy density intermediate between those of (001) and (111)B.

The balance of energy can thus be written as a function of the NS volume V

$$E = E_S + E_V = \gamma_S S - R e_{2D} V = \gamma_S e k_V^{-2/3} V^{2/3} - R e_{2D} V, \quad (5)$$

$$\text{where } k_V = \frac{V}{w^3} = \left(3e(1-t^2) - (1+2t^3-3t^2) \frac{\tan \alpha}{\tan \beta} \right) \frac{\tan \alpha}{12}. \quad (6)$$

R is displayed in Fig. 2(b) for the shapes defined by $e \geq \tan \alpha / \tan \beta$ (i.e., $e \geq 1$ here) and $1 < t \leq 0$. First, we report in Fig. 2(c) the energy density E/V , for a particular NS volume, of 100 nm^3 . A $\gamma_{(114)B}$ of $49.0 \text{ meV}/\text{Å}^2$ is considered. For the truncation ratio $t = 1$ (2D morphology), the balance of energy is null. For t fixed lower than 1, E/V decreases as the shape evolves from very long wires (large e) to shorter ones (small e). There is a truncation ratio ($t = 0.81$ here), above which the NSs are too flat to be more stable than the 2D morphology. For more truncated NSs ($t < 0.81$), the efficiency of the elastic relaxation can overcome the surface contribution, so that the balance of energy can be negative. These behaviors are the same as for isotropic surface energy (i.e., if $\gamma_{(114)A}$ and $\gamma_{(114)B}$ had been equal). However, unlike it would happen with isotropic surface energy, here the minimum value of E/V does not correspond to isotropic islands but to wires with e varying from 45 for $t = 0.9$ to 20 for $t = 0$. E/V increases again as e gets closer to 1, which can be attributed to the increasing role of the B facets in E_S . Considering the anisotropic surface energy, the equilibrium shape is thus a compromise between wire-like shapes (favored by the anisotropic surface energy) and island-like shapes (favored by the elastic relaxation). For the small 100 nm^3 volume, the equilibrium shape is $e = 24$ and $t = 0.154$ [red dot in Fig. 2(c)], corresponding to a 0.6 nm -high, 87 nm -long and 3.7 nm -wide wire.

Then, we determined numerically e^{ES} and t^{ES} the elongation and truncation ratios of the equilibrium shape as a function of the NS volume. They are displayed in Fig. 3 for $\gamma_{(114)B}$ values of 49.0 and 54.0 meV/A². At low volumes, the equilibrium shape is an elongated truncated structure. As V increases, the truncation progressively disappears [Fig. 3(a)] and the elongation slowly decreases [Fig. 3(b)]. While the truncation disappears fully, the elongation ratio collapses and after a transitory regime, islands are achieved (here, with e^{ES} around 3). Further evolution with increasing V is a slow reduction of e^{ES} towards 1. For both $\gamma_{(114)B}$ values, same trends are observed. However, the

lower the $\gamma_{(114)B}$ value, the lower the volume where the transition occurs, and the smoother the transition becomes.

These trends can be interpreted by the change in the surface and strain contributions with volume. At the early growth stage, the strain energy is small, and the surface energy plays a key role. As seen in Fig. 2(c), the most stable shapes are elongated and partially truncated wires, conciliating moderate elastic relaxation and small surface cost, thanks to the predominance of A facets. In a large volume limit, the equilibrium shape corresponds to structures allowing high strain relaxation, i.e., more isotropic full pyramids rather than elongated wires. Figures 3(c) and 3(d) display the relaxation factor R^{ES} and the effective surface energy γ_s^{ES} corresponding to the equilibrium shape as a function of the volume. The change from the surface driven to strain driven regime is highlighted by the abrupt change in the slope of R^{ES} and γ_s^{ES} .

The height, the width and the length of NS equilibrium shapes (h^{ES} , w^{ES} , and L^{ES} , respectively) are then reported in Fig. 4. The sizes calculated before and after the shape transition are close to the experimental data (Table I) for wires and islands, respectively. Indeed, for $\gamma_{(114)B}$ of 54.0 meV/A², the NS sizes drastically change from $h^{ES} = 5$ nm, $w^{ES} = 28$ nm, and $L^{ES} = 450$ nm to $h^{ES} = 9$ nm, $w^{ES} = 54$ nm and $L^{ES} = 155$ nm, while the volume only changes from 32 000 nm³ to 35 000 nm³, corresponding, respectively, to the end of the surface driven regime and the beginning of the strain driven regime. For $\gamma_{(114)B}$ of 49.0 meV/A², the transition is smoother and occurs at about 2500 nm³ ($h^{ES} = 3$ nm, $w^{ES} = 17$ nm and $L^{ES} = 100$ nm).

Complementary calculations were performed considering (111)B ($\beta = 54.7^\circ$) instead of (114)B facets and $\gamma_{(111)B}$ between 50 and 56 meV/A². A clear transition (not shown) from elongated truncated structures to more isotropic and untruncated islands also occurs, with same orders of magnitude of height and width at the transition as with (114)B facets.

Finally, since the gain of elastic energy E_V scales with $(\Delta a/a)^2$ [from Eq. (2)], a higher mismatch leads to an island-like regime at

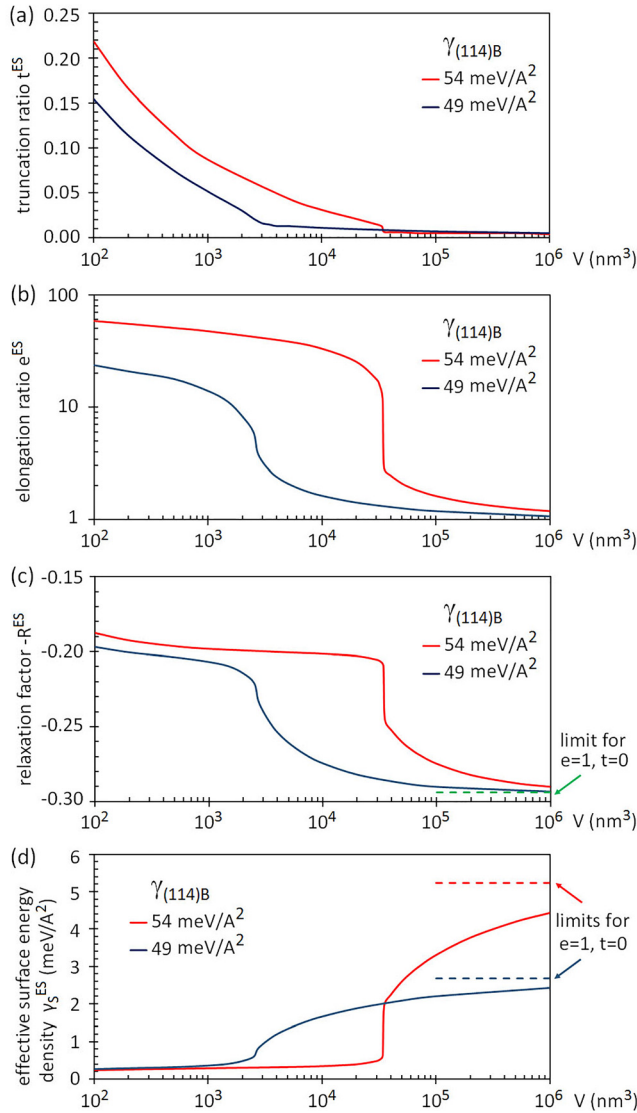


FIG. 3. Equilibrium shape as a function of the NS volume V , determined for $\alpha = \beta = 19.5^\circ$, $\gamma_{(001)} = 47.0$ meV/A², $\gamma_{(114)A} = 44.5$ meV/A², $\gamma_{(114)B} = 49.0$ meV/A² and 54 meV/A² (blue and red lines, respectively). (a) Truncation ratio t^{ES} . (b) Elongation ratio e^{ES} . (c) Relaxation factor R^{ES} . The dashed line corresponds to the limit (0.294 from FEM) achieved for $e = 1$ and $t = 0$. (d) Effective surface energy density γ_s^{ES} . The dashed lines are the limits calculated for $e = 1$ and $t = 0$ [from Eq. (4)].

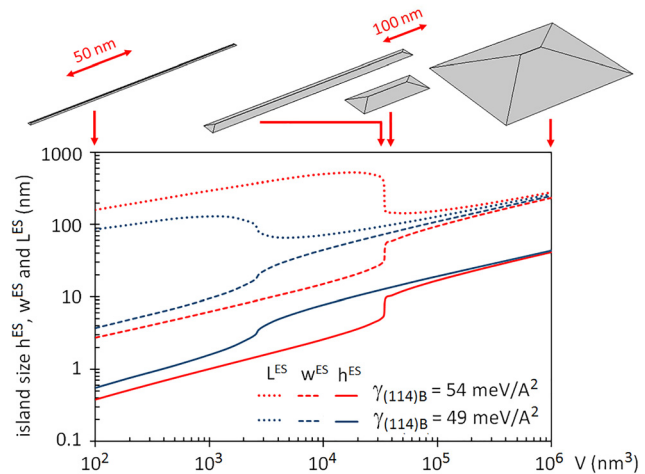


FIG. 4. Height h^{ES} , length L^{ES} , and width w^{ES} of the equilibrium shape as a function of the NS volume V , determined for $\alpha = \beta = 19.5^\circ$, $\gamma_{(001)} = 47.0$ meV/A², $\gamma_{(114)A} = 44.5$ meV/A², $\gamma_{(114)B} = 49.0$ meV/A² and 54 meV/A² (blue and red lines, respectively). The drawn equilibrium shapes are for $\gamma_{(114)B} = 54$ meV/A².

smaller volumes than found here in the InAs/InP moderate mismatch system. In particular, our model predicts an island-like regime at small NS volumes in the InAs/GaAs system, as observed experimentally. As an illustration, with the same small volume (100 nm^3) and surface energies as in Fig. 2(c), the 7.2% misfit of the InAs/GaAs system leads to an untruncated island-like equilibrium shape ($t^{\text{ES}} = 0$; $e^{\text{ES}} = 1.8$) corresponding to a 1.6 nm-high, 16 nm-long and 9 nm-wide island. Conversely, reducing the lattice mismatch (that can occur, for instance, by intermixing between InAs and the preceding alloy buffer layer) should favor the wire-like regime.

In a combined work comprising AFM measurements of the InAs NS grown by MBE and calculations of the NS thermodynamic stability, we provide evidence for a shape transition in InAs/InP (001) material system islanding. As InAs NS facets are non-equivalent along the [110] and $\bar{1}10$ directions, at low volumes the anisotropy of the surface energy drives the formation of particular crystal facets, and thus elongated structures are energetically favorable. This mechanism is favored by the existence of a very stable surface (114)A (from DFT, we found the surface energy of its $\alpha 2(2 \times 1)$ reconstruction around $41 \text{ meV}/\text{Å}^2$) and by the low lattice mismatch in the InAs/InP system (3.2%), which enhances the surface effects compared to systems with a higher mismatch (as in InAs/GaAs). For higher NS volumes, a more isotropic shape is found to be preferable due to more efficient strain relaxation. The NS sizes for which our model predicts this shape transformation (from 3–5 nm to 8–10 nm in height and from 20–30 nm to 60–70 nm in width) are in very good agreement with experiments. It shows that despite the relatively high growth rate used, at any stage of the size island evolution, the island shape is close to that minimizing the balance between surface and elastic energies, i.e., the equilibrium shape for this volume. To go further, STM analysis of facet structures and their changes with kinetic factors (growth rate, arsenic pressure, and substrate temperature) is required.

REFERENCES

- ¹S. Pes, C. Paranthoën, C. Levallois, N. Chevalier, C. Hamel, K. Audo, G. Loas, S. Bouhier, C. Gomez, J.-C. Harmand, S. Bouchoule, H. Folliot, and M. Alouini, *Opt. Express* **25**, 11760 (2017).
- ²Y. Y. Ding, F. Gao, H. H. Yuan, Z. R. Lv, and T. Yang, *IEEE Photonics Technol. Lett.* **30**, 1234 (2018).
- ³M. A. Shemis, M. T. A. Khan, E. Alkhazraji, A. M. Ragheb, M. A. Esmail, H. Fathallah, K. K. Qureshi, S. Alshebeili, and M. Z. M. Khan, *Opt. Commun.* **410**, 680 (2018).
- ⁴M. Z. M. Khan, T. K. Ng, and B. S. Ooi, *Prog. Quantum Electron.* **38**, 237 (2014).
- ⁵A. Ponchet, A. Le Corre, H. L'Haridon, B. Lambert, and S. Salaün, *Appl. Phys. Lett.* **67**, 1850 (1995).
- ⁶P. J. Poole, J. McCaffrey, R. L. Williams, J. Lefebvre, and D. Chithrani, *J. Vac. Sci. Technol., B* **19**, 1467 (2001).
- ⁷J. P. Reithmaier, A. Somers, S. Deubert, R. Schwertberger, W. Kaiser, A. Forchel, M. Calligaro, P. Resneau, O. Parillaud, S. Bansropun, M. Krakowski, R. Alizon, D. Hadass, A. Bilenca, H. Dery, V. ikhelashvili, G. Eisenstein, M. Gioannini, I. Montrosset, T. W. Berg, M. van der Poel, J. Mørk, and B. Tromborg, *J. Phys. D* **38**, 2088 (2005).
- ⁸C. Gilfert, E.-M. Pavelescu, and J. P. Reithmaier, *Appl. Phys. Lett.* **96**, 191903 (2010).
- ⁹L. González, J. M. García, R. García, F. Briones, J. Martínez-Pastor, and C. Ballesteros, *Appl. Phys. Lett.* **76**, 1104 (2000).
- ¹⁰A. Stintz, T. J. Rotter, and K. J. Malloy, *J. Cryst. Growth* **255**, 266 (2003).
- ¹¹D. Jung, D. J. Ironside, S. R. Bank, A. C. Gossard, and J. E. Bowers, *J. Appl. Phys.* **123**, 205302 (2018).
- ¹²G. Costantini, A. Rastelli, C. Manzano, R. Songmuang, O. G. Schmidt, K. Kern, and H. von Känel, *Appl. Phys. Lett.* **85**, 5673 (2004).
- ¹³F. M. Ross, R. M. Tromp, and M. C. Reuter, *Science* **286**, 1931 (1999).
- ¹⁴J. Tersoff and F. K. LeGoues, *Phys. Rev. Lett.* **72**, 3570 (1994).
- ¹⁵H. R. Gutiérrez, R. Magalhães-Paniago, J. R. R. Bortoleto, and M. A. Cotta, *Appl. Phys. Lett.* **85**, 3581 (2004).
- ¹⁶P. Miska, J. Even, C. Platz, B. Salem, T. Benyattou, C. Bru-Chevalier, G. Guillot, G. Bremond, K. Moumanis, F. H. Julien, O. Marty, C. Monat, and M. Gendry, *J. Appl. Phys.* **95**, 1074 (2004).
- ¹⁷V. Swaminathan and A. T. Macrander, *Materials Aspects of GaAs and InP, Based Structures* (Prentice-Hall, Inc., Englewood Cliffs, New Jersey, 1991).
- ¹⁸A. Ponchet, D. Lacombe, L. Durand, D. Alquier, and J.-M. Cardonna, *Appl. Phys. Lett.* **72**, 2984 (1998).
- ¹⁹I. W. Yeu, J. Park, G. Han, C. S. Hwang, and J.-H. Choi, *Sci. Rep.* **7**, 10691 (2017).
- ²⁰C. Ratsch, W. Barvosa-Carter, F. Grosse, J. H. G. Owen, and J. J. Zinck, *Phys. Rev. B* **62**, R7719 (2000).
- ²¹N. Moll, M. Scheffler, and E. Pehlke, *Phys. Rev. B* **58**, 4566 (1998).
- ²²J. Márquez, P. Kratzer, and K. Jacobi, *J. Appl. Phys.* **95**, 7645 (2004).
- ²³I. Lucci, S. Charbonnier, M. Vallet, P. Turban, Y. Léger, T. Rohel, N. Bertru, A. Létoublon, J.-B. Rodriguez, L. Cerutti, E. Tournié, A. Ponchet, G. Patriarche, L. Pedesseau, and C. Cornet, *Adv. Funct. Mater.* **28**, 1801585 (2018).
- ²⁴M. Imura, H. Kurohara, Y. Masui, T. Asano, T. Kitada, S. Shimomura, and S. Hiayamizu, *J. Vac. Sci. Technol. B* **23**, 1158 (2005).